Available online at www.sciencedirect.com
SCIENCE DIRECT
Journal of Solid State Chemistry 179 (2006) 2182–2189
JOURNAL OF SOLID STATE CHEMISTRY
www.elsevier.com/locate/jssc

Evaluation of the acid properties of porous zirconium-doped and undoped silica materials

D. Fuentes-Perujo[a], J. Santamaría-González[a], J. Mérida-Robles[a], E. Rodríguez-Castellón[a], A. Jiménez-López[a], P. Maireles-Torres[a,*], R. Moreno-Tost[b], R. Mariscal[b]

[a]*Departamento de Química Inorgánica, Cristalografía y Mineralogía (Unidad Asociada al ICP-CSIC), Facultad de Ciencias, Universidad de Málaga, Campus de Teatinos, 29071 Málaga, Spain*

[b]*Instituto de Catálisis y Petroleoquímica, CSIC, c/ Marie Curie 2, Campus Cantoblanco, 28049 Madrid, Spain*

Received 31 January 2006; received in revised form 6 April 2006; accepted 9 April 2006
Available online 25 April 2006

Abstract

A series of porous silica and Zr-doped silica molecular sieves, belonging to the MCM-41 and MSU families, were prepared and characterized by X-ray diffraction (XRD), X-ray photoelectron spectroscopy (XPS) and N_2 adsorption at 77 K. Their acid properties have been evaluated by NH_3-TPD, adsorption of pyridine and deuterated acetonitrile coupled to FT-IR spectroscopy and the catalytic tests of isopropanol decomposition and isomerization of 1-butene. The acidity of purely siliceous solids were, in all cases, very low, while the incorporation of Zr(IV) into the siliceous framework produced an enhancement of the acidity. The adsorption of basic probe molecules and the catalytic behaviour revealed that Zr-doped MSU-type silica was more acidic than the analogous Zr-MCM-41 solid, with a similar Zr content. This high acidity observed in the case of Zr-doped silica samples is due to the presence of surface zirconium atoms with a low coordination, mainly creating Lewis acid sites.
© 2006 Elsevier Inc. All rights reserved.

Keywords: Zirconium oxide; Porous silica; MCM-41; Isopropanol decomposition; 1-butene isomerization

1. Introduction

An important breakthrough in the field of mesoporous solids was the discovery and subsequent development of the so-called M41S family. Considerable literature is now available dealing the synthesis, characterization and applications of mesoporous molecular sieves [1–7]. This is mainly because their uniform pores, high specific surface areas and tunable acid–base and redox properties make them excellent candidates to find wide utility in catalysis and sorption. Therefore, the considerable effort devoted to the developing of the different groups of ordered mesoporous molecular sieves seems to have bridged the gap between microporous (zeotypes) and macroporous (amorphous materials) solids.

It is well known that siliceous materials exhibit a very low acidity associated to surface silanol groups, but the incorporation of heteroatoms such as B, Al, Ti, Fe, Zr, Ga, into the mesoporous silica framework can enhance the acid properties, which can be controlled systematically by proper choice of the type and the amount of the doping element [8–10]. Acid solids are thoroughly used in heterogeneous catalysis, as both acid catalysts and supports.

The study of the acid–base properties of solids has been the objective of many investigations, extending from the use of spectroscopic methods to the evaluation of the catalytic behaviour in different test reactions, as well as the desorption of probe molecules followed by temperature-programmed techniques [11–16].

The majority of papers dealing the acid characterization of mesoporous materials have been devoted to mesoporous aluminosilicates [17–22]. Thus, the study of the effect of pore size on Al stability and acidity of mesoporous

*Corresponding author. Fax: +34 952137534.
E-mail address: maireles@uma.es (P. Maireles-Torres).

0022-4596/$ - see front matter © 2006 Elsevier Inc. All rights reserved.
doi:10.1016/j.jssc.2006.04.018

Al-MCM-41 has revealed that the stability of tetrahedral aluminum is higher at smaller pore sizes [18]. These authors conclude that the isomerization selectivity of 2-methyl-2-pentene, as acidity test, not only depends on the pore size but also on the Si/Al molar ratio of the mesoporous catalysts, among other design variables, and a more complete physical characterization is needed to shed light on the structure–reactivity relationships.

Recently, Zhai et al. [23] have demonstrated that AlMSU-2 are more active in the catalytic cracking of 1,3,5-triisopropylbenzene than AlMCM-41 with a similar Si/Al molar ratio. This better performance is attributed to the wormhole framework structure which three-dimensional character allows a more readily access of guest molecules to the inner reactive sites.

However, in recent years, much attention is being also focused on the study of zirconium-doped mesoporous silica materials, not only concerning their synthesis [24–28] but also their applications in the adsorption of C_{60} fullerene [29], as catalysts in oxidation reactions with hydrogen peroxide in liquid phase [30], in the vapor synthesis of alkylindoles [31], and catalyst support in reactions such as the Fischer–Tropsch synthesis [32], hydrogenation and ring-opening of tetralin [33], gas-phase hydrogenation of acetonitrile [34] and SCR of NO with ammonia [35].

Thus, zirconium-doped mesoporous silicas have also demonstrated to be active as acid catalysts in isopropanol decomposition, where the catalytic activity in propylene production is proportional to the amount of zirconium incorporated into the silica network [27,28].

In this paper, we describe the results concerning the evaluation of the acid properties of Zr-doped and undoped mesoporous silica, belonging to the MCM-41 and MSU families, by using the adsorption of different basic molecule probes (ammonia, pyridine and deuterated acetonitrile), and the catalytic tests of isopropanol decomposition and isomerization of 1-butene. Previously, the materials have been characterized by X-ray diffraction (XRD), N_2 adsorption at 77 K and X-ray photoelectron spectroscopy (XPS).

2. Experimental

2.1. Preparation of catalysts

Chemicals were supplied by Aldrich and used as received. Zirconium-containing mesoporous MCM-41-type silica was prepared by adding appropriate amounts tetraethoxysilane ethanol solution and zirconium *n*-propoxide to an aqueous solution of hexadecyltrimethylammonium bromide (25 wt%), previously stirred at 353 K for 30 min. The surfactant/($SiO_2 + ZrO_2$) molar ratio was 0.5. The pH was adjusted to 10 by addition of an aqueous solution of tetramethylammonium hydroxide (25 wt%), and the resulting gels were stirred at room temperature for 4 days. Solid products were recovered by centrifugation, washed with ethanol, dried at 343 K, and then calcined in air at 823 K for 6 h (1 K min^{-1} heating rate) in order to remove the surfactant. A material with a Si/Zr molar ratio of 5 was prepared, MCMSiZr5 [27]. The MCM-41 silica was obtained by the same procedure but without the addition of zirconium.

MSU derivatives were prepared according to the following procedure [28]: (i) 5.1 mmol of zirconyl chloride octahydrate, 2.5 mmol of sodium hydroxide and 11.9 mmol of sodium silicate ($Na_2Si_3O_7$) were added, under vigorous stirring, to 100 ml of a 0.1 M Triton X100 solution prepared by dissolving the appropriate amount of surfactant in a 0.4 M HCl solution (Triton/(Si + Zr) molar ratio of 0.24). After stirring during 5 days at room temperature, the solid was separated by filtration, washed with distilled water and dried at 333 K. The porous MSUSiZr7 was obtained after calcination at 823 K, (ii) the purely siliceous sample, MSUSi, was prepared by following the same synthesis procedure but without adding zirconium to the reaction medium.

2.2. Characterization

Powder XRD patterns were recorded on a Siemens D5000 diffractometer using Cu-$K\alpha$ radiation and a graphite monochromator. Nitrogen adsorption–desorption isotherms at 77 K were obtained using an automatic Micromeritics ASAP 2020, previously outgassing the samples at 473 K and 1×10^{-2} Pa overnight. BET specific surface areas were evaluated using 0.162 nm^2 as the cross-sectional area of the adsorbed nitrogen molecule. Pore size distributions were calculated with the Cranston and Inkley method for cylindrical pores [36].

X-ray photoelectron spectra were obtained using a Physical Electronics PHI 5700 spectrometer with non-monochromatic Mg-$K\alpha$ radiation (300 W, 15 kV, 1253.6 eV). High-resolution spectra were recorded at 45° take-off-angle by a concentric hemispherical analyzer operating in the constant pass energy mode at 29.35 eV, using a 720 mm diameter analysis area. Under these conditions the Au $4f_{7/2}$ line was recorded with 1.16 eV FWHM at a binding energy of 84.0 eV. Charge referencing was done against adventitious carbon (C 1*s* 284.8 eV). The pressure in the analysis chamber was maintained $< 5 \times 10^{-6}$ Pa. PHI ACCESS ESCA-V6.0 F software package was used for acquisition and data analysis. A Shirley-type background was subtracted from the signals. Recorded spectra were always fitted using Gauss–Lorentz curves in order to determine more accurately the binding energy of the different element core levels.

The total acidity was evaluated by temperature programmed desorption of ammonia (NH_3-TPD). The samples were first heated in a He flow at 823 K to remove adsorbed surface species, before adsorbing ammonia at 373 K. NH_3-TPD was carried out between 373 and 823 K, at 10 K min^{-1}, and then maintaining at 823 K for 30 min, with on-line gas chromatographic analysis (Shimadzu GC-14A) by TCD.

Infrared spectra of the chemisorbed pyridine and deuterated acetonitrile (CD_3CN) were recorded at room temperature on a Fourier transform infrared Nicolet 5 ZDX at a resolution of $4\,cm^{-1}$. Each spectrum was averaged over 128 scans. Self-supporting wafers (ca. $10\,mg\,cm^{-2}$) were evacuated under vacuum at 823 K during 1 h in an infrared vacuum cell equipped with greaseless stopcocks and KBr windows. After introducing the pyridine and CD_3CN at room temperature (650 Pa in both cases), the fraction of physically adsorbed molecules were outgassed at room temperature for 5 min. To study the stability of absorption bands, degassing at different temperatures was performed. The net infrared spectra of chemisorbed CD_3CN were obtained after subtracting the background spectrum of the solid.

The catalytic decomposition of isopropanol was used as a test reaction for the study of the effective acidity. A fixed-bed tubular glass reactor working at atmospheric pressure was used for a solid charge of 30 mg without dilution (0.2–0.3 mm particle size). Samples were pretreated at 473 K in a helium flow for 3 h ($60\,ml\,min^{-1}$). Isopropanol was fed into the reactor by flowing He (dried through a molecular sieve, flow rate $25\,cm^3\,min^{-1}$) through a saturator–condenser at 303 K, which gives rise to a constant isopropanol flow of 7.5 vol%. None of the samples showed diffusion restrictions. The reaction products were analyzed by an on-line gas chromatograph (Shimadzu GC-14A) provided with a FID and a fused silica capillary column SPB1.

The catalytic isomerization of 1-butene was performed in a tubular glass flow microreactor. The samples (130 mg with a particle size of 0.2–0.3 mm) were pretreated for 2 h in a He flow at 673 K ($30\,ml\,min^{-1}$), and experiments were carried out at this temperature. The 1-butene was at 5 vol% concentration in He and the total flow was $32\,cm^3\,g^{-1}$. The reactant 1-butene and the reaction products were analyzed on-line in a gas chromatograph (Shimadzu GC-14B) equipped with a wide-bore $KCl/AlCl_3$ column. For this reaction, the distribution of *n*-butenes is near equilibrium and, consequently, the conversion is defined as the ratio [(products-*n*-butenes)/1-butene feed] × 100.

3. Results and discussion

3.1. Characterization of catalysts

The powder XRD patterns of the siliceous and Zr-doped silica materials, after calcination at 823 K for removing the organic structure-directing agent, only exhibit a low-angle diffraction peak, characteristic of the MCM-41 and MSU structures (Fig. 1). The absence of other higher-order reflections in the XRD patterns can be attributed to the existence of a limited long-range order, due to the low temperature (298 K) used in the synthesis of these porous materials. Moreover, the incorporation of heteroatoms into the silica framework decreases the intensity and broadens the main diffraction peak. No diffraction peaks corresponding to the presence of bulk ZrO_2 crystallites were observed in the high-angle region.

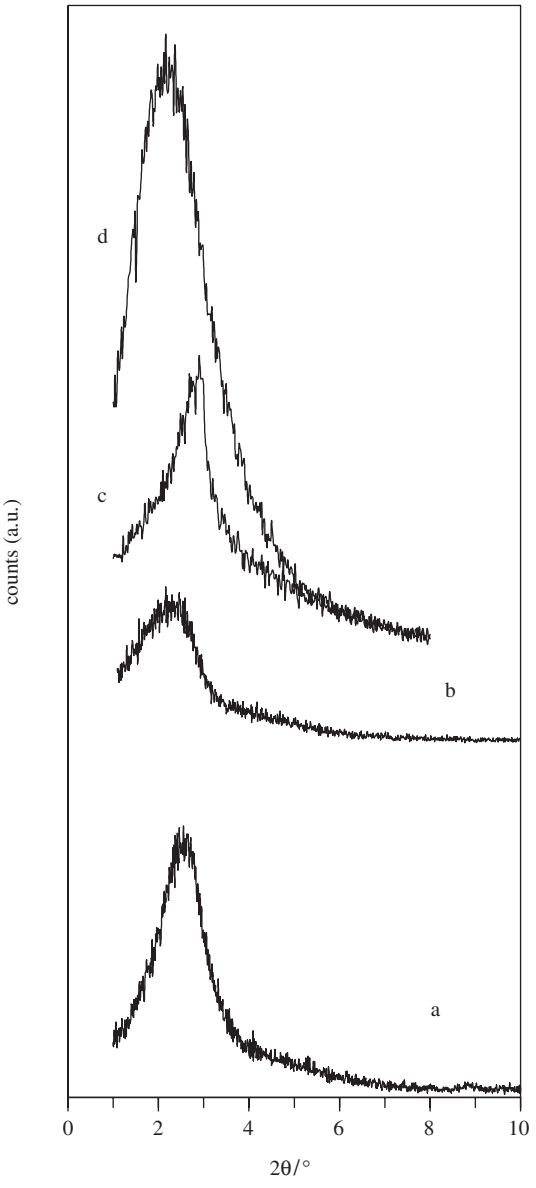

Fig. 1. Powder X-ray diffraction patterns of: (a) MCMSi, (b) MCMSiZr5, (c) MSUSi and (d) MSUSiZr7 materials.

Table 1
Textural characteristics of the porous solids

Sample	S_{BET} (m^2/g)	V_p (cm^3/g)	d_p av[a] (nm)
MCMSi	749	0.567	2.9
MCMSiZr5	444	0.350	3.0
MSUSi	705	0.346	1.8
MSUSiZr7	708	0.364	1.9

[a]Average pore size values deduced by using the Cranston and Inkley method [26].

The porous nature of the prepared materials was evaluated by N_2 sorption at 77 K (Table 1). The corresponding isotherms of the MCM-41 materials are Type IV in the IUPAC classification, and in all cases the typical inflexion at low relative pressure was observed (Fig. 2). As expected, the MSU-type solids show isotherms which can be classified as intermediated between Type I and IV, pointing to the presence of a super-microporous network, favoured by the use of diluted surfactant solutions and low pH in their synthesis [37,38].

The pore size distributions, determined by the Cranston and Inkley method for cylindrical pores, corroborate the different nature of the porous framework (Fig. 3). They are narrow and the maximum average pore diameter is centred between 1.6 and 2.8 nm. It can be observed that the incorporation of heteroatoms into the mesoporous MCM-41 silica shifts the maximum pore sizes to higher values, being the smallest pores observed for MSU-type materials, accordingly to their adsorption–desorption isotherms.

The results concerning the surface characterization of the porous solids, performed by XPS analyses, are displayed in Table 2. Although, in general, this technique is used to study the surface characteristics of solids, by considering that the photoelectron has an escape depth up to ca. 4 nm, comparable to the wall thickness in the studied porous materials, XPS could provide information about bulk composition. In the case of zirconium-doped porous silica, the observed surface Si/Zr molar ratios are higher than the nominal values used in the synthesis. This fact has been previously observed and it has been attributed to the different hydrolysis and condensation rates of the zirconium and silicon precursors. Moreover, these materials exhibit an asymmetric O 1*s* signal, which can be deconvoluted into a low-energy component close to 531 eV and other peak at ca. 532.5 eV (see Table 2). The contribution of the former peak increases with the zirconium content, and by considering that the O 1*s* B.E. in zircon, $ZrSiO_4$, appears at 531.4 eV, that could be assigned to oxygen atoms belonging to the coordination sphere of zirconium (Fig. 4).

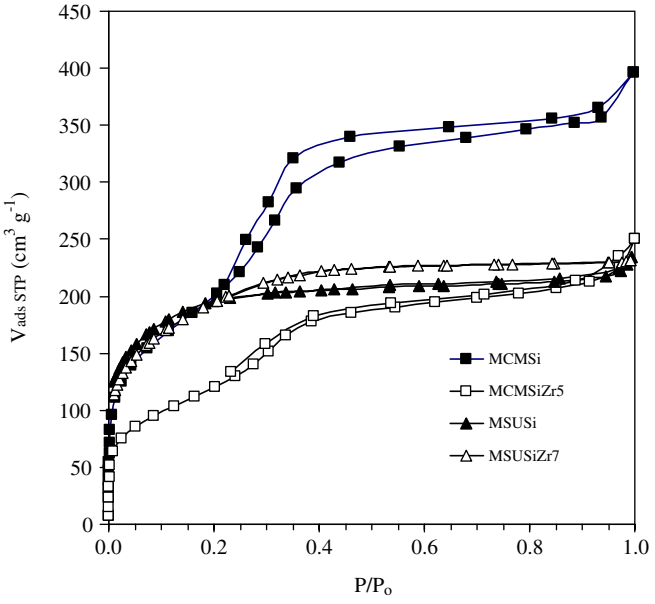

Fig. 2. Adsorption–desorption isotherms of N_2 at 77 K of the different porous solids.

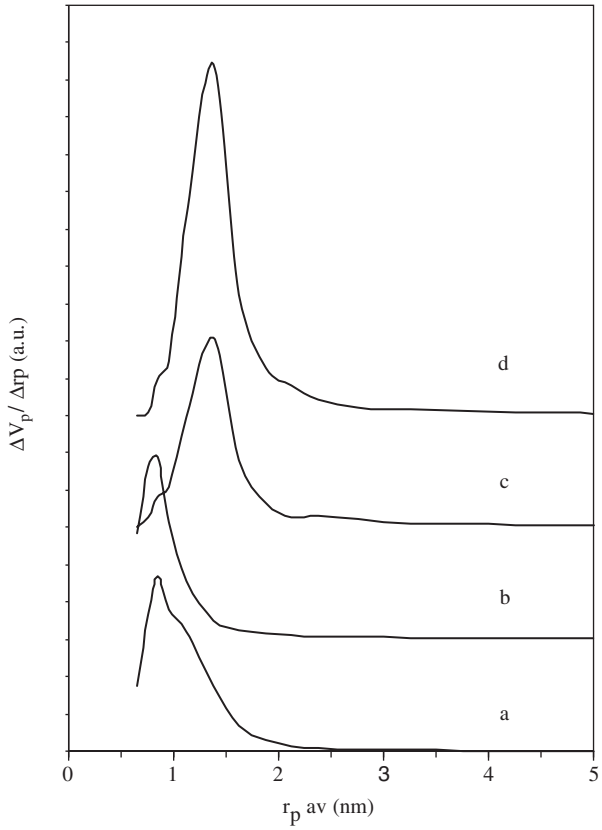

Fig. 3. Pore size distributions, as determined by the Cranston and Inkley method, of (a) MSUSiZr7, (b) MSUSi, (c) MCMSiZr5, and (d) MCMSi materials.

It is well known that the incorporation of heteroatoms, such as Zr(IV), into a siliceous framework gives rise to surface acid sites, which are active in different acid-catalysed reactions. The temperature-programmed desorption of ammonia is a widely used method to evaluate the concentration and strength of acid centres of solid oxides [12]. These studies have demonstrated that substitution of Si(IV) by heteroatoms leads to the formation of Brønsted and Lewis acid sites of different type and strength on the surface of mesoporous solids. Ammonia desorption profiles between 373 and 823 K are very broad, and under isothermal conditions at 823 K, desorption of ammonia is still detected. In most cases, ammonia is desorbed between 473 and 673 K, indicating the presence of acid sites of weak to medium strength. These results agree well with previous studies, where broad ranges of ammonia desorption temperatures have been reported [21,22].

Fig. 5 displays the amount of desorbed ammonia at different temperature intervals. The amount of desorbed ammonia increases with the presence of zirconium. The

Table 2
Surface characterization, as determined by XPS, of the mesoporous solids

Sample	Binding energy (eV)			Atomic ratio	
	O 1*s*	Si 2*p*	Zr $3d_{5/2}$	O/(Si + Zr)	Si/Zr
MCMSi	533.0	103.8	—	2.12	—
MCMSiZr5	530.9 (16%) 532.6 (84%)	103.2	182.9	2.18	8.9
MSUSi	532.7	103.7	—	2.09	—
MSUSiZr7	530.8 (7%) 532.3 (93%)	103.1	183.3	2.27	9.9

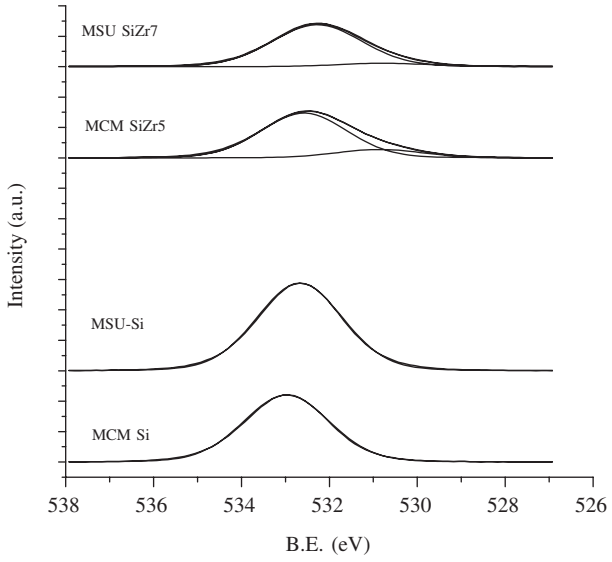

Fig. 4. O 1*s* core level spectra for the studied solids.

order of total acidity, as deduced by NH_3-TPD, is the following: MSUSiZr7 > MCMSiZr5 > MSUSi > MCMSi.

The acidity of the solids has been also studied by means of the adsorption of other probe basic molecules such as pyridine and CD_3CN coupled to FT-IR spectroscopy.

The spectra recorded after the adsorption of pyridine at room temperature on mesoporous solids, outgassed at different temperatures, are shown in Fig. 6. The mesoporous silica only displays a band at 1445 cm^{-1} due to the pyridine weakly bonded by hydrogen bonds to OH groups, which disappears after evacuation at 393 K. MSUSi is not included in the Fig. 6 because its spectrum is similar to that of MCMSi. Therefore, as expected, these pure silica solids do not present noticeable acidity.

The presence of heteroatoms increases the acidity. The spectrum of the MCMSiZr5 solid shows a band at 1445 cm^{-1}, which reveals the presence of Lewis acid sites [39]. This Lewis acidity is originated by the presence of Zr(IV) deficiently coordinated on the surface of the walls [31]. In addition to the acidity of Lewis type, this sample also presents a band at 1547 cm^{-1} characteristic of the Brønsted acid sites. This band stays up to 523 K. These Brønsted sites are associated with Zr–OH and bridged Zr–O(H)–Si groups [28]. On the other hand, the band associated to Lewis acid sites diminishes its intensity with the temperature, although Lewis acid sites are still present at 623 K. Thus, this zirconium-doped solid shows mainly Lewis acid sites.

The MSUSiZr7 sample exhibits both Lewis and Brønsted acid sites, being similar to MCMSiZr5.

The acetonitrile is also a probe molecule widely used to elucidate the acid strength of solids since the band due to the vibration ν_{CN} is very sensible to the interaction between the acid sites and the acetonitrile. Nevertheless, this vibration band is masked by the Fermi resonance resulting from the ν_{CN} band and the $\delta_{s(CH3)} + \nu_{C-C}$ combination band. In order to overcome this limitation, deuterated acetonitrile (CD_3CN) was used. When CD_3CN is adsorbed, the ν_{CN} band moves towards higher frequencies depending on the magnitude of interaction between the CN group and the solid. Thus, valuable information about the strength of the Lewis acid sites can be obtained from the position of coordinated CD_3CN in the region 2300–2350 cm^{-1}, since the frequency normally increases with the strength of Lewis acid sites.

In Fig. 7 the IR spectra after the adsorption of CD_3CN at room temperature and after different periods of evacuation are shown, so as at 375 and 473 K for MCM SiZr5 and MSUSiZr7 are more acid samples. The mesoporous pure silica display a band of tension solely of $C \equiv N$ at 2276 cm^{-1}, which can be attributed to the presence of molecules of CD_3CN weakly interacting to OH groups [40,41], decreasing its intensity with the evacuation time.

The MCMSiZr5 presents, in addition to the band at 2274 cm^{-1}, another new band centred at 2305 cm^{-1} corresponding to CD_3CN adsorbed on Lewis acid sites. Moreover, this band even remains when CD_3CN is evacuated at 473 K. These results are in agreement with those obtained from pyridine adsorption.

Finally, the MSUSiZr7 sample displays two bands centred at 2305 cm^{-1}, with a shoulder to 2296, and at 2272 cm^{-1}. This last band is typical of the adsorption of CD_3CN on OH groups. The band centred at 2305 cm^{-1} seems to be the contribution of the adsorption of the CD_3CN on two different types of Lewis acid sites. The degasification at room temperature provokes that the

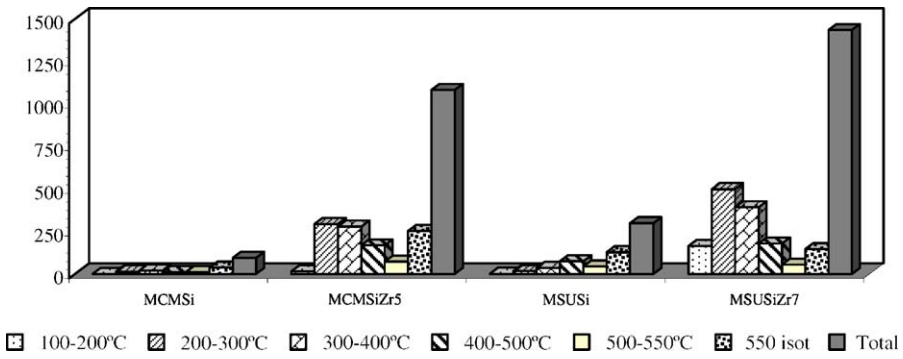

Fig. 5. Histograms of temperature-programmed desorption of ammonia.

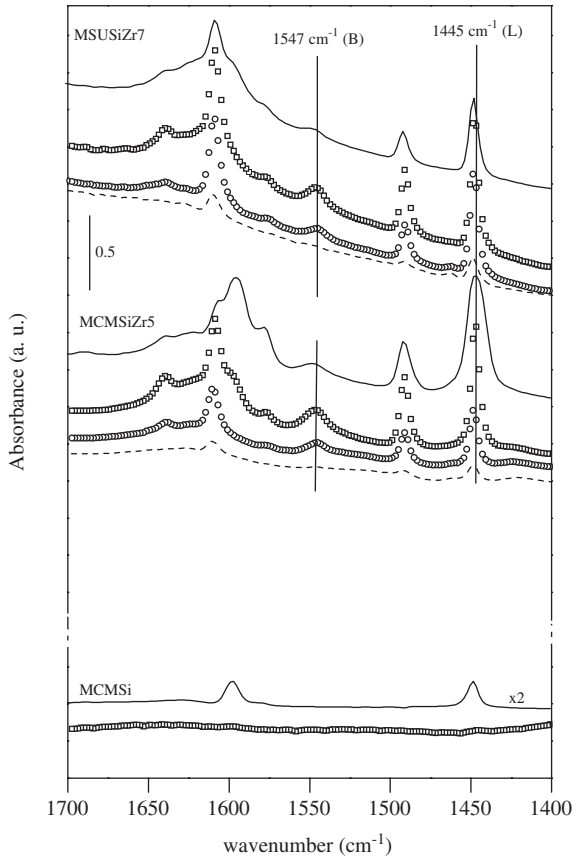

Fig. 6. IR spectra of adsorbed pyridine, after evacuation at different temperatures: (—) room temperature; (□) 393 K; (○) 523 K and (— — —) 623 K.

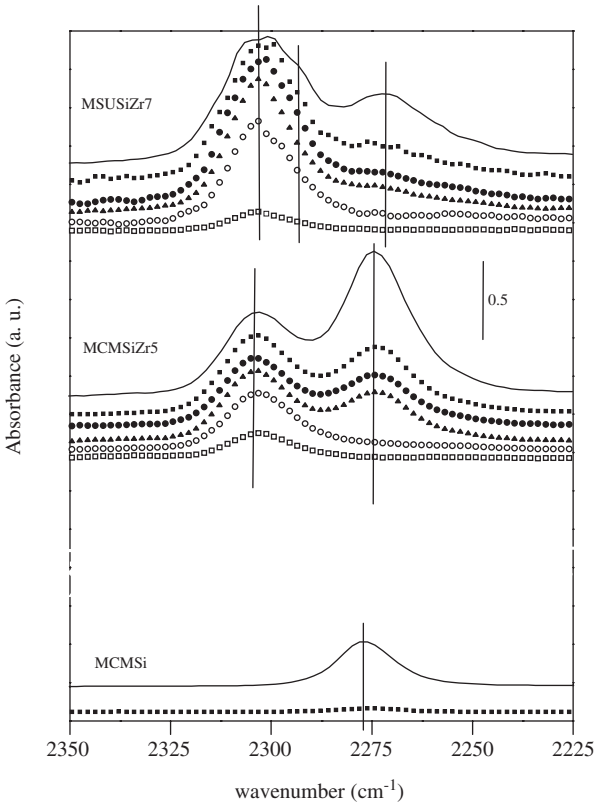

Fig. 7. IR spectra of deuterated acetonitrile adsorbed on the different porous solids, after evacuation at different times and temperatures: (—) room temperature; (■) 10′; (●) 20′; (▲) 30′; (○) 373 K and (□) 473 K.

intensity of the band at 2272 cm^{-1} diminished progressively, whereas the band at 2305 cm^{-1} is only affected when the solid is evacuated at 473 K.

Therefore, the adsorption of the basic probe molecules, pyridine and CD_3CN, on these samples gives rise to similar results. Thus, the porous silica solids do not show noticeable acidity. Among the substituted porous silica, the MCMSiZr5 sample shows an important number of acid sites, basically Lewis acid sites and they are thermally resistant. The MSUSiZr7 sample exhibits a similar behaviour to MCMSiZr5 sample.

3.2. Catalytic results

In order to study the effective acidity of the different porous solids under dynamic experimental conditions, the decomposition of isopropanol has been used as acidity test. The dehydration of isopropanol to propylene and/or diisopropyl ether requires the presence of acid centres, whereas the dehydrogenation to acetone occurs on basic or redox sites. It should be mentioned the fact that dehydration activity is always observed at lower temperatures than dehydrogenation. Concerning the mechanism implied in the dehydrogenation of isopropanol, there have been postulated the dehydration via the formation a carbonium

ion mechanism, as well as via a trans-elimination reaction or E_2 mechanism, being the later that which is mostly supported by experimental data [42].

In all cases, during the catalytic runs, propylene and acetone have been the only products detected in the isopropanol decomposition, and neither diisopropyl ether nor polymerization products were observed.

Porous silica materials, MCMSi and MSUSi, as expected from the previous results, only show activity in the decomposition of isopropanol at 623 K, where propylene and acetone are formed (Fig. 8). The presence of the dehydrogenation product, acetone, is only observed at this high reaction temperature.

Isopropanol undergoes dehydration over the Zr-doped silica, showing these samples a very high selectivity toward propylene. Diisopropyl ether was not observed in any case. The most active sample is that which has previously shown the higher acidity by using basic probe molecules, MUSiZr7.

Finally, we have also used the isomerization of 1-butene as another catalytic measure of acidity. The products of this reaction can be classified as: (i) double bond isomerization (*cis*- and *trans*-2-butenes), (ii) skeletal isomerization products (isobutene), (iii) hydrogenated products (*n*-butane and isobutane), (iv) cracking compounds (lower alkanes), (v) surface carbon residues and (vi) butadiene and higher molecular weight compounds. Therefore, there are two types of isomerization: a double bond or a methyl migration. Double bond isomerization does not need very strong acidity ($0.82 > H_R > -4.04$), and the *cis*/*trans*-2-butenes ratio gives insights into the acid (*cis*/*trans* < 1) or basic (*cis*/*trans* > 1) nature of the catalyst, while the methyl shift only takes place on strong acid sites ($H_R < -6.63$). If we assume that the double bond isomerization occurs on all acid sites and the methyl migration only on those acid centres which exhibit an acidity above some threshold, the selectivity ratio isobutene/(*cis* + *trans*)-2-butenes will be an approximate measure of the distribution of strong acid site density into the total acid site density. These values are compiled in Table 3, and it can be inferred from these that the MCMSiZr5 and MSUSiZr7 are the more acidic samples, with values higher than 0.10. However, porous silicas do not produce isobutene, confirming the weakness of the acid sites present on the surface of these solids.

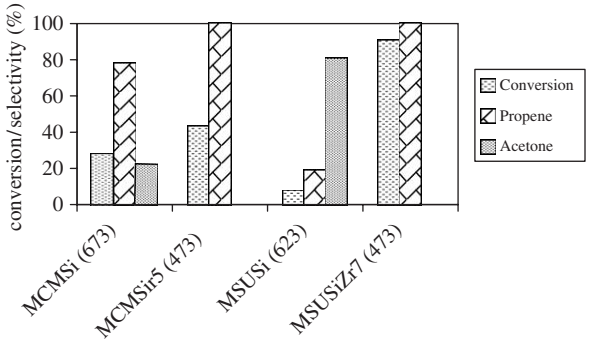

Fig. 8. Conversion and selectivities in the isopropanol decomposition. The reaction temperature is indicated for each sample.

On the other hand, unfortunately no relevant information can be obtained from the (*cis*/*trans*)-2-butene ratio because, under the experimental conditions used in this work, the higher levels of conversion favour the subsequent isomerization reaction of *cis*-2-butene to the thermodynamically more stable *trans*-2-butene, thus lowering the observed *cis*/*trans* ratio. The results in the isomerization of 1-butene reveal that porous silicas, MCMSi and MSUSi, are barely active, with conversion lower than 10%, according to the data deduced from NH_3-TPD and adsorption of pyridine and CD_3CN molecules. However, the introduction of zirconium into the silica framework creates acid sites which are able to catalyse the conversion of 1-butene, with values close to 70%, and (*cis*/*trans*)-2-butene ratios near to 0.75. In all cases, after 2 h of time-on-stream, no deactivation of the catalysts was observed (Fig. 9).

It has been postulated that the elimination step from a tert-butyl carbenium ion to give isobutene would be an acid-base reaction which need a basic site on the catalyst surface to locate the proton. Thus, this step would be favoured on weakly acidic catalysts carrying basic oxygens, more than on strongly acidic catalysts, and this fact explains the high selectivity to isobutene of alumina-based catalysts [43]. However, the presence of very strong acid sites might lead the catalytic reaction toward the formation of dimerization and oligomerization products, as well as cracking compounds. The data displayed in Table 3 indicate that high percentages of cracking compounds, mainly propylene, are detected on the MSUSi catalyst, which can be attributed to the use of high reaction temperatures, and never due to the presence of strong acid

Table 3
1-butene isomerization data on porous materials at 673 K (except 773 K for MSUSi)

Sample	Conversion (%)	Selectivity (%)				*i*/(*c* + *t*)
		cis-2-C_4H_8	*trans*-2-C_4H_8	*iso*-C_4H_8	Cracking	
MCMSi	7.7	46	46.5	0	0.3	0
MCMSiZr5	72.9	37.4	50.2	9.0	2.4	0.10
MSUSi	0.22	38.9	32.9	0	14.4	0
MSUSiZr7	74.2	35.7	48.6	10.9	3.7	0.13

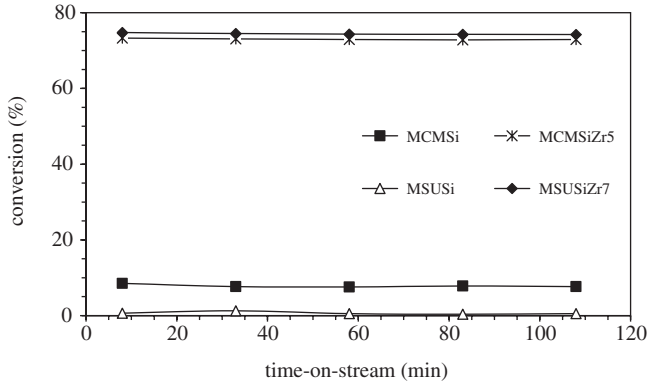

Fig. 9. Evolution of the conversion of 1-butene as a function of time-on-stream ($T = 673$ K).

sites, because they were not detected by adsorption of CD_3CN coupled to IR spectroscopy.

4. Conclusions

Therefore, it can be concluded that results obtained in the acid characterization of solids by using static methods, such as NH_3-TPD and adsorption of basic probes molecules (pyridine, deuterated acetonitrile) coupled to IR spectroscopy, agree very well with those obtained by dynamic studies, as demonstrated in the case of the decomposition of isopropanol and isomerization of 1-butene, where the most active catalyst is that which exhibits the highest acidity. In all cases, the incorporation of zirconium into the silica framework creates acid sites, which amount and effective acidity are higher in the case of MSU-type solids.

Acknowledgments

We are gratefully acknowledged to the Ministerio de Ciencia y Tecnología (Spain) for funding this work under the Project MAT2003-08348.

References

[1] J.S. Beck, J.C. Vartuli, W.J. Roth, M.E. Leonowicz, C.T. Kresge, K.D. Schmitt, C.T.W. Chu, D.H. Olson, E.W. Sheppard, S.B. McCullen, J.B. Higgins, J.L. Schlenker, J. Amer. Chem. Soc. 114 (1992) 10834.
[2] A. Monnier, F. Schuth, Q. Huo, D. Kumar, D. Margolese, R.S. Maxwell, G.D. Stucky, M. Krishnamurty, P. Petroff, A. Firouzi, M. Janicke, B.F. Chmelka, Science 261 (1993) 1299–1303.
[3] A. Sayari, Chem. Mater. 8 (1996) 1840–1852.
[4] A. Corma, Chem. Rev. 97 (1997) 2373–2419.
[5] U. Ciesla, F. Schüth, Micropor. Mesopor. Mater. 27 (1999) 131–149.
[6] T.J. Barton, L.M. Bull, W.G. Klemperer, D.A. Loy, B. McEnaney, M. Misono, P.A. Monson, G. Pez, G.W. Sherer, J.C. Vartuli, O.M. Yaghi, Chem. Mater. 11 (1999) 2633–2656.
[7] D. Trong On, D. Desplantier-Giscard, C. Danumah, S. Kaliaguine, Appl. Catal. A 253 (2003) 545–602.
[8] H. Kosslick, G. Lischke, H. Landmesser, B. Parlitz, W. Storek, R. Fricke, J. Catal. 176 (1998) 102–114.
[9] H. Landmesser, H. Kosslick, U. Kurschner, R. Fricke, J. Chem. Soc. Faraday Trans. 94 (1998) 971–977.
[10] A. Tuel, Micropor. Mesopor. Mater. 27 (1999) 151–169.
[11] E. Brunner, Catal. Today 38 (1997) 361–376.
[12] G. Busca, Phys. Chem. Chem. Phys. 1 (1999) 723–736.
[13] A. Corma, H. García, Catal. Today 38 (1997) 257–308.
[14] M. Guisnet, in: B. Imelick (Ed.), Catalysis by Acids and Bases, Elsevier, Amsterdam, 1985, p. 45.
[15] J.L.G. Fierro, Stud. Surf. Sci. Catal. 57 (1990) B67–B143.
[16] G. Bagnasco, J. Catal. 159 (1996) 249–252.
[17] A. Corma, V. Fornés, M.T. Navarro, J. Pérez-Pariente, J. Catal. 148 (1994) 569–574.
[18] X. Feng, J.S. Lee, J.W. Lee, J.Y. Lee, D. Wei, G.L. Haller, Chem. Eng. J. 64 (1996) 255–263.
[19] R. Mokaya, W. Jones, Z. Luan, M.D. Alba, J. Klinowski, Catal. Lett. 37 (1996) 113–120.
[20] A. Liepold, K. Roos, W. Reschetilowski, Chem. Eng. Sci. 51 (1996) 3007–3012.
[21] H. Kosslick, G. Lischke, B. Parlitz, W. Storek, R. Fricke, Appl. Catal. 184 (1999) 49–60.
[22] H. Kosslick, H. Landmesser, R. Fricke, J. Chem. Soc., Faraday Trans. 93 (1997) 1849–1854.
[23] S. Zhai, J. Zheng, X. Shi, Y. Zhang, L. Dai, Y. Shan, M. He, D. Wu, Y. Sun, Catal. Today 93–95 (2004) 675–680.
[24] M.I. Occelli, S. Biz, A. Auroux, Appl. Catal. A 183 (1999) 231–239.
[25] W.H. Zhang, J.L. Shi, L.Z. Wang, D.S. Yan, Mater. Lett. 46 (2000) 25–38.
[26] X.X. Wang, F. Lefebvre, J. Patarin, J.M. Basset, Micropor. Mesopor. Mater. 42 (2001) 269–276.
[27] E. Rodríguez-Castellón, A. Jiménez-López, P. Maireles-Torres, D.J. Jones, J. Rozière, M. Trombetta, G. Busca, M. Lenarda, L. Storaro, J. Solid State Chem. 175 (2003) 159–169.
[28] A. Infantes-Molina, J. Mérida-Robles, P. Maireles-Torres, E. Finocchio, G. Busca, E. Rodríguez-Castellón, J.L.G. Fierro, A. Jiménez-López, Micropor. Mesopor. Mater. 75 (2004) 23–32.
[29] I. Piwonski, J. Zarjac, D.J. Jones, J. Rozière, S. Partyka, J. Mater. Chem. 8 (1998) 17–18.
[30] S. Gontier, A. Tuel, Appl. Catal. A 143 (1996) 125–135.
[31] A.O. Bianchi, M. Campanati, P. Maireles-Torres, E. Rodríguez-Castellón, A. Jiménez-López, A. Vaccari, Appl. Catal. A 220 (2001) 105–112.
[32] M. Wei, K. Okabe, H. Arakawa, Y. Teraoka, Catal. Commun. 5 (2004) 597–603.
[33] E. Rodríguez-Castellón, J. Mérida-Robles, L. Díaz, P. Maireles-Torres, D.J. Jones, J. Rozière, A. Jiménez-López, Appl. Catal. A 260 (2004) 9–18.
[34] M.C. Carrión, B.R. Manzano, F.A. Jalón, I. Fuentes-Perujo, P. Maireles-Torres, E. Rodríguez-Castellón, A. Jiménez-López, Appl. Catal. A 288 (2005) 34–42.
[35] R. Moreno-Tost, E. Rodríguez-Castellón, A. Jiménez-López, J. Mol. Catal. A 248 (2006) 126–134.
[36] R.W. Cranston, F.A. Inkley, Adv. Catal. 9 (1957) 143–154.
[37] C. Boissière, A. Larbot, A. Van der Lee, P.J. Kooyman, E. Prouzet, Chem. Mater. 12 (2000) 2902–2913.
[38] A. Léonard, J.L. Blin, P.A. Jacobs, P. Grange, B.L. Su, Micropor. Mesopor. Mater. 63 (2003) 59–73.
[39] X. Xu Wang, F. Lefebvre, J. Patarin, J.M. Basset, Micropor. Mesopor. Mater. 42 (2001) 269–276.
[40] B. Pawelec, S. Damyanova, R. Mariscal, J.L.G. Fierro, I. Sobrados, J. Sanz, L. Petrov, J. Catal. 223 (2004) 86–97.
[41] S. Damyanova, L. Dimitrov, R. Mariscal, J.L.G. Fierro, L. Petrov, I. Sobrados, Appl. Catal. A 256 (2003) 183–197.
[42] A. Gervasini, J. Fenyvesi, A. Auroux, Catal. Lett. 43 (1997) 219–228.
[43] M. Trombetta, G. Busca, S. Rossini, V. Piccoli, U. Cornaro, A. Guercio, R. Catani, R.J. Willey, J. Catal. 179 (1998) 581–596.